

## ORIGINAL RESEARCH ARTICLE

# Study on catalytic properties of graphene/molybdenum sulfide under near-infrared light irradiation

Huan Zhang<sup>1,2</sup>, Shouqing Liu<sup>1,2\*</sup>

<sup>1</sup> School of Chemistry, Biology and Materials Engineering, Suzhou University of Science and Technology, Suzhou, Jiangsu 215009, China. E-mail: Shouqing\_liu@163.com

<sup>2</sup> Jiangsu Key Laboratory of Environmental Functional Materials, Suzhou, Jiangsu 215009, China.

### ABSTRACT

Graphene/MoS<sub>2</sub> hybrid material was prepared by the hydrothermal method. The hybrid material was characterized by X-ray diffraction spectrum, Raman spectra, transmission electron microscope and UV-vis-NIRS. It was used as a near-infrared photocatalyst to catalyze and degrade Rhodamine B (RhB). The results showed that when the concentration of the RhB solution was 50.0 mg·L<sup>-1</sup>, the pH value of the solution was 7, the volume of the solution was 50.0 mL, the amount of G/MoS<sub>2</sub> catalyst was 0.05 g and near-infrared radiation was carried out for 3 h, the degradation rate of RhB in the 50 mL solution reached 96.5%. When MoS<sub>2</sub> was used as the photocatalyst, the degradation rate of RhB was only 75.5%. After 5 times of recycling, the catalytic efficiency of the hybrid photocatalyst was still more than 90%, indicating that the catalyst is very stable.

**Keywords:** G/MoS<sub>2</sub>; Hybrid Catalyst; Near-Infrared Light; Photocatalysis

### ARTICLE INFO

Received: 24 October 2021  
Accepted: 29 December 2021  
Available online: 12 January 2022

### COPYRIGHT

Copyright © 2022 Huan Zhang, *et al.*  
doi: 10.24294/ace.v5i1.1402  
EnPress Publisher LLC. This work is licensed under the Creative Commons Attribution-NonCommercial 4.0 International License (CC BY-NC 4.0).  
<https://creativecommons.org/licenses/by-nc/4.0/>

## 1. Introduction

The use of solar energy to solve environmental energy originated in 1972 when Fujishima used TiO<sub>2</sub> optoelectrode to electrolyze water for hydrogen production<sup>[1]</sup>. Then Carey reported that TiO<sub>2</sub> photocatalytic oxidation was used to eliminate the toxicity of polychlorinated diphenol in 1976<sup>[2]</sup>. Since then, the degradation of environmental pollutants by solar energy has rapidly become a research hotspot. However, TiO<sub>2</sub> can only use ultraviolet accounting for about 4% of solar energy to dope TiO<sub>2</sub><sup>[3-5]</sup> and develop new catalysts such as Fe<sub>2</sub>O<sub>3</sub>, WO<sub>3</sub> and Bi<sub>2</sub>WO<sub>6</sub><sup>[6,7]</sup>. Although the utilization of visible light is partially solved, infrared accounting for nearly 50% of solar energy needs to be developed and utilized. While visible light photocatalysis continues to be concerned, in recent years, people have begun to promote the research frontier of photocatalysis to the utilization of near-infrared light. It has been reported that hydrogen was prepared by photocatalysis with In<sub>2</sub>TiO<sub>5</sub> as catalyst and near-infrared light as driving force<sup>[8]</sup>; g-C<sub>3</sub>N<sub>4</sub> was sensitized with phthalocyanine and hydrogen was prepared by near-infrared light radiation<sup>[9]</sup>; Tang, *et al.* used NaYF<sub>4</sub>:Yb and Tm as up-conversion materials to convert near-infrared light into ultraviolet that can be absorbed and utilized by TiO<sub>2</sub>, and degraded methylene blue through TiO<sub>2</sub> photocatalysis<sup>[10]</sup>; Li, *et al.* formed a composite nanostructure with carbon quantum dots and Cu<sub>2</sub>O, which can degrade organic dyes by near-infrared photocatalysis<sup>[11]</sup>.

In recent years, two-dimensional materials have attracted extensive attention because of their good optical and electrical properties<sup>[12]</sup>. MoS<sub>2</sub> is similar to graphene and has a two-dimensional planar structure<sup>[13]</sup>. The hydrogen production property of MoS<sub>2</sub> (a semiconductor photocatalyst) under visible light radiation has been studied<sup>[14–21]</sup>. In the application of near infrared, literature only reported the research of MoS<sub>2</sub> for photothermal drug releasing in the treatment of cancer<sup>[22]</sup>. As a semiconductor material, MoS<sub>2</sub> has an indirect band gap of 1.29 eV<sup>[23]</sup>. The theoretical absorption sideband can extend to 961 nm and can absorb near infrared, which provides a scientific foundation for near-infrared photocatalysis.

On the other hand, graphene (G) is a hot spot in the study of carbon materials in recent years. It is a two-dimensional monatomic layer material, and its basic structural unit is a six-membered ring<sup>[24,25]</sup>. Each carbon atom in G-structure provides a p orbital electron to form an delocalized  $\pi$  bond, and the P electron can move freely, making G have good conductivity<sup>[26]</sup>. The combination of G and MoS<sub>2</sub> is expected to prepare the G/MoS<sub>2</sub> hybrid photocatalyst with catalytic activity for near infrared, and to make full use of solar energy.

This paper adopted the hydrothermal method to prepare the G/MoS<sub>2</sub> photocatalyst and used RhB as a simulated pollutant to study the law of near-infrared photocatalytic degradation of RhB.

## 2. Experiment

### 2.1 Preparation of a G/MoS<sub>2</sub> nanocomposite semiconductor material

#### 2.1.1 Preparation of MoS<sub>2</sub>

Add 1.21 g NaMoO<sub>4</sub>·2H<sub>2</sub>O (0.005 mol) and 1.56 g (NH<sub>2</sub>)<sub>2</sub>CS (0.020 mol) into a 100 mL beaker; stir until they are completely dissolved, and then transfer them to a polytetrafluoroethylene hydrothermal reactor. Add deionized water to 80% of the total volume of the reactor, seal the reactor, heat it to 200 °C and react for 24 hours. Then cool the sample at room temperature and wash it with deionized water to remove the soluble substances. The black solid powder was obtained and dried in an oven at 40 °C for 6 h to obtain the MoS<sub>2</sub> semi-

conductor material.

#### 2.1.2 Synthesis of graphite oxide (GO)

Accurately weigh 2.0 g of graphite and 1.0 g of NaNO<sub>3</sub> into a 200 mL beaker and add 50 mL of concentrated H<sub>2</sub>SO<sub>4</sub>, then add 6.0 g of KMnO<sub>4</sub>, and react for 2 h at a temperature lower than 20 °C. Then raise the temperature to 35 °C for 35 min; add a certain amount of deionized water to the reaction system, stir continuously for 20 min, then reduce the residual potassium permanganate with 60 mL of 5% H<sub>2</sub>O<sub>2</sub> until the solution turns bright yellow. Filter it while it is hot, wash with 5% HCl and deionized water until there is no SO<sub>4</sub><sup>2-</sup>, and fully dry in a 60 °C vacuum drying oven to obtain GO sample for standby.

#### 2.1.3 Preparation of G/MoS<sub>2</sub>

In the process of synthesizing MoS<sub>2</sub>, G/MoS<sub>2</sub> nano hybrid materials with different G contents were obtained by adding GO with mass fractions of 1%, 3%, 5%, 7% and 9% respectively into the mixed solution of NaMoO<sub>4</sub>·2H<sub>2</sub>O and (NH<sub>2</sub>)<sub>2</sub>CS and carrying hydrothermal reaction at 200 °C for 24 h.

#### 2.1.4 Preparation of the RhB solution

Weigh 0.1 g of RhB and fix the volume to 100 mL to obtain the RhB solution with a concentration of 1 mg·mL<sup>-1</sup>.

#### 2.1.5 Characterization analysis

The samples were characterized by an X-ray diffractometer (XRD, D/max 2500 pC), a transmission electron microscope (TEM, Tecnai G220), a fourier transform infrared spectrometer (Spectrum BX, PerkinElmer Ltd, USA), an ultraviolet/visible/near infrared spectrophotometer (UV-Vis, U-4100) and a Raman spectrometer (LabRAMHR800, France).

### 2.2 Photocatalytic reaction

Use a 100 mL round-bottom beaker as a photoreactor and wrap the four walls of the beaker with tin foil paper to prevent ultraviolet and visible light from entering the reaction system. A cut-off filter with  $\lambda > 780$  nm is covered on the beaker mouth to ensure that only near-infrared light radiation enters the photoreactor. Place a 300 W UV-Vis lamp above

the reactor, add a certain amount of catalysts to the RhB solution of a certain concentration, magnetically stir, sample every 20 minutes during the reaction, centrifuge, and determine the absorbance of RhB at 554 nm with an UV-Vis spectrophotometer to calculate the degradation rate of RhB.

$$\text{Degradation rate of RhB} = (1 - C_i/C_0) \times 100\% = (1 - A_i/A_0) \times 100\%$$

In the formula,  $C_0$  is the initial concentration of RhB;  $A_0$  is the absorbance of the initial solution,  $C_i$  is the concentration of remaining RhB, and  $A_i$  is the absorbance of remaining RhB.

### 3. Results and discussion

#### 3.1 X-ray powder diffraction characterization

**Figure 1** shows the XRD powder diffraction spectra of samples of MoS<sub>2</sub>, GO, G and G/MoS<sub>2</sub>. The diffraction peaks at  $2\theta = 14.2^\circ$ ,  $33.5^\circ$ ,  $39.5^\circ$  and  $59.0^\circ$  correspond to (002), (100), (103) and (110) crystal plane indexes of MoS<sub>2</sub> respectively. The diffraction peaks of MoS<sub>2</sub> and G/MoS<sub>2</sub> are consistent with the standard spectrum (JCPDS37-1492). Therefore, it can be determined that the obtained sample is MoS<sub>2</sub> (space group:  $P_3^6/mmc$ )<sup>[27]</sup>.

Curve (b) in **Figure 1** is the diffraction spectrum of GO. The characteristic diffraction peak of GO appears at  $8.5^\circ$ , indicating that a large number of oxygen-containing functional groups are introduced into the graphite interlayer<sup>[28,29]</sup>. Curve (c) is the diffraction pattern of graphene after hydrothermal reduction. Compared with curve (b), it can be seen that the original diffraction peak at  $8.5^\circ$  disappears and a diffraction peak appears at  $2\theta = 24.4^\circ$ . The peak shape is dispersed and wide, indicating that after hydrothermal treatment, the functional groups on the GO surface are gradually reduced to obtain the assembly structure formed by single or few G-layers. The integrity of the crystal structure decreases and the degree of disorder increases<sup>[28,30]</sup>.

Curve (d) is the G/MoS<sub>2</sub> diffraction spectrum. Compared with MoS<sub>2</sub>, the crystal plane index of MoS<sub>2</sub> appears at the same position, and the characteristic diffraction peak of G appears at  $25.4^\circ$ . The displacement of the peak position may be caused by

the introduction of MoS<sub>2</sub>.

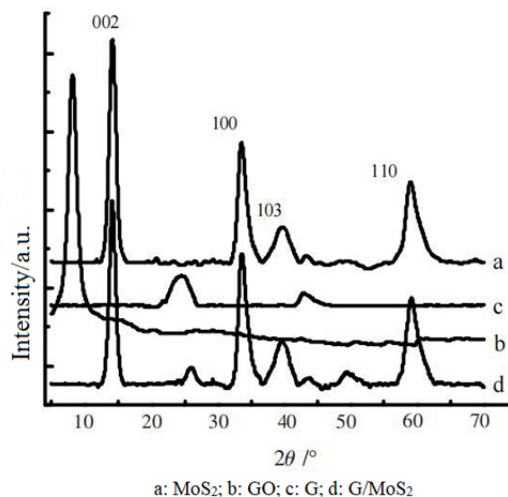


**Figure 1.** X-ray powder diffraction spectra of samples.

#### 3.2 Raman spectra characterization

MoS<sub>2</sub> unit cells are stacked according to hexagonal symmetry and belong to  $D_{6h}^4$  space group ( $P_3^6/mmc$ ). According to the symmetry, MoS<sub>2</sub> has four Raman active vibration modes:  $E_{2g}^2$ ,  $E_{1g}$ ,  $E_{2g}^1$ ,  $A_{1g}$ <sup>[31]</sup>. It can be seen from **Figure 2(a)** that the Raman peaks at  $385\text{ cm}^{-1}$  and  $408\text{ cm}^{-1}$  belong to  $E_{2g}^1$  and  $A_{1g}$  vibration respectively, which further indicates that the prepared sample is MoS<sub>2</sub>.

**Figure 2(b)** and **Figure 2(c)** represent the Raman spectra of GO and GO treated by hydrothermal reduction respectively. GO and reduced-GO materials have two important characteristic bands near wave numbers of  $1335\text{ cm}^{-1}$  and  $1600\text{ cm}^{-1}$ , namely D-band and G-band. G-band is the  $E_{2g}$  vibration mode of GO, which corresponds to the  $sp^2$  hybridization of carbon atoms. D-peak is generated by the stretching vibration of  $sp^3$  hybrid C-C single bond, which is a measure of defects and disorder of G. The intensity ratio ( $I_D/I_G$ ) of the two is often used to characterize the disorder degree of the structure. By calculating, the  $I_D/I_G$  of GO is 1.27 and that of G is 1.88, showing that G after hydrothermal treatment becomes a single-layer or few layers of G-sheets; the average size of  $sp^2$  plane domain decreases and the disorder degree increases<sup>[32]</sup>.

**Figure 2(d)** is the Raman spectrum of G/MoS<sub>2</sub>. The characteristic  $E_{2g}^1$  and  $A_{1g}$  vibration modes of MoS<sub>2</sub> appear. At the same time, the Raman peaks of G of  $1600\text{ cm}^{-1}$  and  $1335\text{ cm}^{-1}$  also appear, which further indicates the successful recombination of G

and MoS<sub>2</sub>.

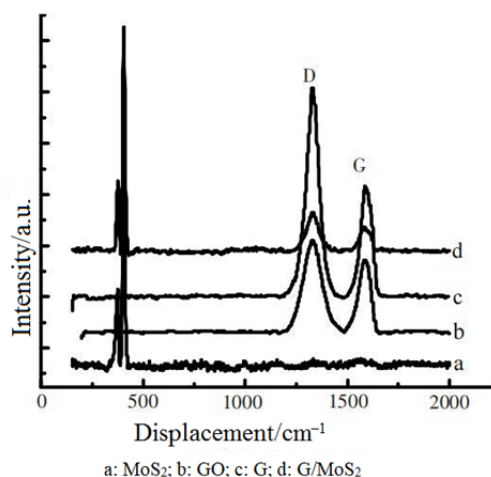


Figure 2. Raman spectra.

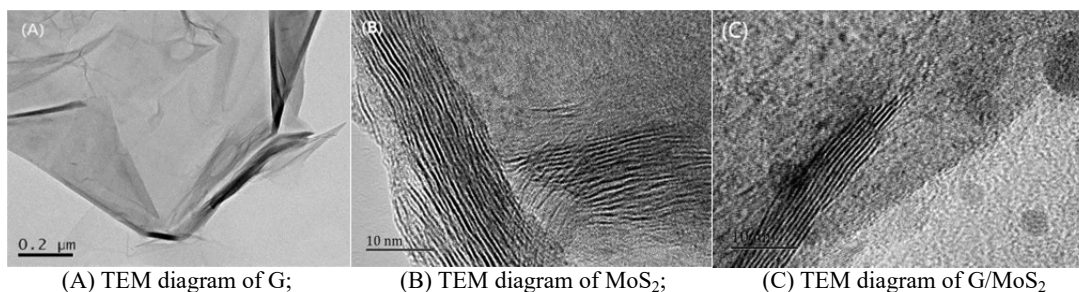


Figure 3. TEM diagrams of samples.

### 3.4 UV-vis-infrared reflectance characterization

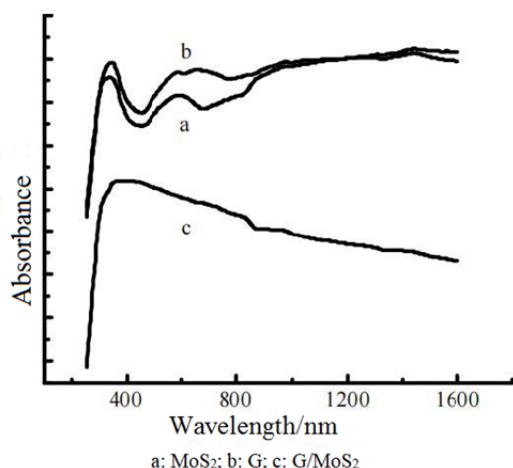


Figure 4. UV-vis-near-infrared reflectance spectra of samples.

Figure 4 shows the reflectance spectra of MoS<sub>2</sub>, G/MoS<sub>2</sub> and G samples. It can be seen from Figure 4 that the two samples not only have a strong absorption peak near 300 nm, but also have an obvious absorption peak between 500–850 nm, so the samples have good absorption performance in the ultraviolet and visible regions. Because MoS<sub>2</sub> supports G, the absorption band of composite

### 3.3 Transmission electron microscope

Figure 3(A) shows the TEM diagram of G. It can be seen from Figure 3 that G is in a sheet structure, which also shows that G is synthesized by this method. Figure 3(B) is the TEM diagram of MoS<sub>2</sub> with a layer spacing of 0.629 nm, which is the surface spacing of (002), indicating that the material is a MoS<sub>2</sub> semiconductor. Figure 3(C) is the TEM diagram of the G/MoS<sub>2</sub> hybrid material. As can be seen from Figure 3, the sub-grain of (002) surface is clearly visible, surrounded by G-carbon material, which shows that G and MoS<sub>2</sub> form a hybrid material with a close structure.

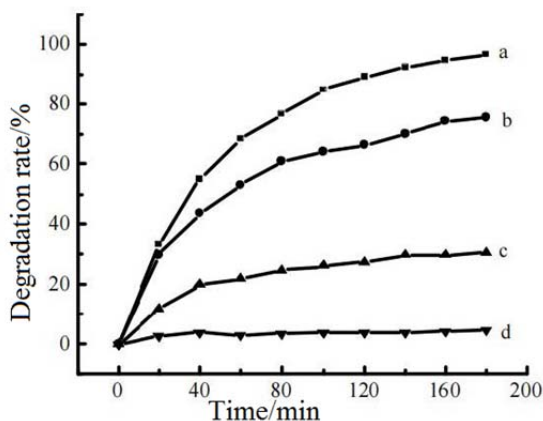
G/MoS<sub>2</sub> has red-shift and has good absorption in the near-infrared region. Therefore, G greatly improves the utilization of solar energy by the catalyst.

## 4. The degradation experiment of RhB

### 4.1 Photocatalytic degradation of RhB

Figure 5 shows the curve of G/MoS<sub>2</sub> photocatalytic degradation of RhB under near-infrared light radiation. Curve (a) shows that the degradation rate of RhB reaches 96.5% at 3 h. The comparative experiment shows that when there is no hybrid catalyst, even if the RhB solution with the same concentration is directly irradiated by infrared light, the degradation rate of RhB under the same conditions is only 4.3%, as shown in curve (d). Therefore, comparing curve (a) with curve (d), it can be seen that the hybrid material G/MoS<sub>2</sub> plays an important role in the degradation of RhB by near-infrared light. 0.05 g G/MoS<sub>2</sub> catalyst was placed in the same concentration of RhB solution, and 30.3% RhB was adsorbed on the catalyst surface after 3 h

without light, as shown in curve (c). Under the same conditions, when using one group MoS<sub>2</sub> as the catalyst, the degradation rate of RhB is only 75.5%, as shown in curve (b), while the degradation rate of RhB using hybrid catalysts composed of G/MoS<sub>2</sub> is significantly higher than that using MoS<sub>2</sub>. Therefore, G enhances the photocatalysis of MoS<sub>2</sub>.



Degradation conditions: solution volume  $v = 50$  mL, RhB initial concentration  $C = 50$  mg·L<sup>-1</sup>, pH = 7.0. a: 0.05 g G/MoS<sub>2</sub> + infrared light; b: 0.05 g MoS<sub>2</sub> + infrared light; c: 0.05 g G/MoS<sub>2</sub>; d: infrared radiation.

Figure 5. Near-infrared photocatalytic degradation of RhB.

#### 4.2 Effect of the initial RhB concentration

The G/MoS<sub>2</sub> catalyst was used to degrade RhB with different initial concentrations, and the degradation curve was obtained under the same other conditions, as shown in Figure 6. The results show that  $\ln(C_0/C_t)$  has a linear relationship with the reaction time  $t$ , as shown in Figure 7. Therefore, the RhB degradation reaction follows the first-order reaction kinetics. Based on this, the apparent kinetic rate constant  $K_{app}$  can be obtained, whose average value is 0.304 h<sup>-1</sup>.

$$\ln(C_0/C_t) = K_{app}t + b$$

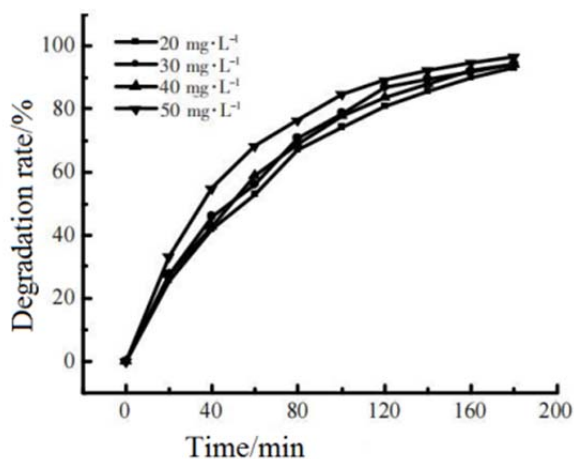


Figure 6. Degrading RhB with different initial concentrations.

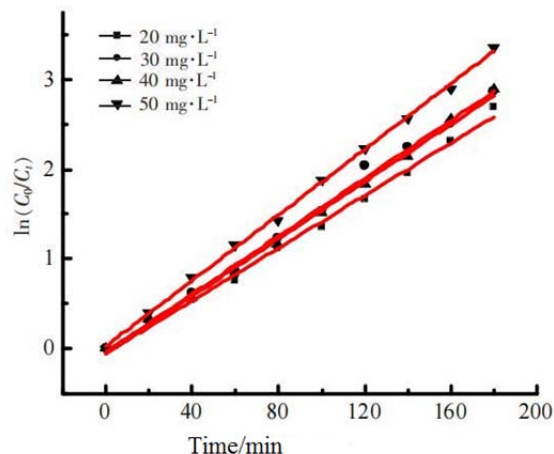


Figure 7. Linear relationship between  $\ln(C_0/C_t)$  and  $t$ .

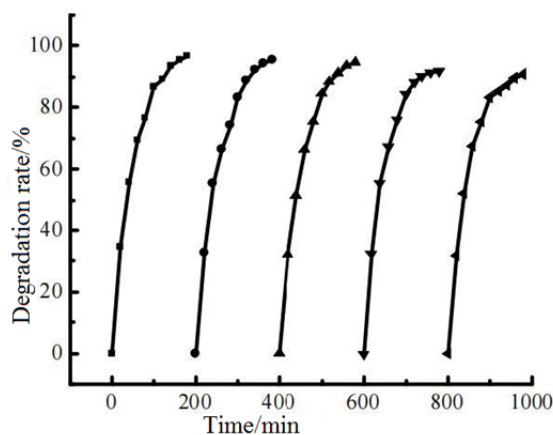


Figure 8. Recycling experiments of G/MoS<sub>2</sub>.

#### 4.3 Stability and reuse of catalyst

The stability of the hybrid catalyst was evaluated by multiple cycle experiments. Figure 8 is the degradation rate curve of the G/MoS<sub>2</sub> catalyst for 5 consecutive times of near-infrared photocatalytic degradation of RhB under near-infrared light radiation. Each experiment lasted for 3 h. After each degradation, the catalyst was obtained by centrifugation and deionized water washing, and then recycled. After five cycles of degradation of RhB, the degradation rate of RhB was still more than 90.6%. This shows that the G/MoS<sub>2</sub> catalyst is relatively stable and can be reused.

### 5. Conclusion

The G/MoS<sub>2</sub> hybrid material was prepared by the hydrothermal method. The hybrid material has photocatalytic properties to near-infrared light. Using this hybrid material as photocatalyst, RhB can be effectively degraded under near-infrared light irradiation. The G/MoS<sub>2</sub> hybrid catalyst was

continuously recycled for 5 times, and the degradation rate of RhB was still more than 90%, indicating that the hybrid catalyst is very stable. The results of this study show that near-infrared light has important application value in the field of environmental protection.

## Conflict of interest

The authors declare that they have no conflict of interest.

## Acknowledgements

This work was supported by the National Natural Science Foundation of China (21576175).

## References

1. Fujishima A, Honda K. Electrochemical photolysis of water at a semiconductor electrode. *Nature* 1972; 238(5358): 37–38.
2. Carey JH, Lawrence J, Tosine HM. Photodechlorination of PCB's in the presence of titanium dioxide in aqueous suspensions. *Bulletin of Environmental Contamination and Toxicology* 1976; 16(6): 697–701.
3. Hoffmann MR, Martin S, Choi W, *et al.* Environmental applications of semiconductor photocatalysis. *Chemical Reviews* 1995; 95(1): 69–96.
4. Rimeh D, Patrick D, Didier R. Modified TiO<sub>2</sub> for environmental photocatalytic applications: A review. *Industrial & Engineering Chemistry Research* 2013; 52(10): 3581–3599.
5. Banerjee S, Pillai SC, Falaras P, *et al.* New insights into the mechanism of visible light photocatalysis. *Journal of Physical Chemistry Letters* 2014; 5(15): 2543–2554.
6. Maneesha M, Doo-man C.  $\alpha$ -Fe<sub>2</sub>O<sub>3</sub> as a photocatalytic material: A review. *Applied Catalysis A: General* 2015; 498(5): 126–141.
7. He R, Cao S, Zhou P, *et al.* Recent advances in visible light Bi-based photocatalysts. *Chinese Journal of Catalysis* 2014; 35(7): 989–1007.
8. Wei D, Yao L, Yang S, *et al.* Band gap Engineering of In<sub>2</sub>TiO<sub>5</sub> for H<sub>2</sub> production under nearinfrared light. *ACS Applied Mater Interfaces* 2015; 7(37): 20761–20768.
9. Zhang X, Yu L, Zhuang C, *et al.* Highly asymmetric phthalocyanine as a sensitizer of graphitic carbon nitride for extremely efficient photocatalytic H<sub>2</sub> production under near-infrared light. *ACS Catalysis* 2013; 4(1): 162–170.
10. Tang Y, Di W, Zhai X, *et al.* NIR-responsive photocatalytic activity and mechanism of NaYF<sub>4</sub>:Yb, Tm@TiO<sub>2</sub> core-shell nanoparticles. *ACS Catalysis* 2013; 3(3): 405–412.
11. Li H, Liu R, Liu Y, *et al.* Carbon quantum dots/Cu<sub>2</sub>O composites with protruding nanostructures and their highly efficient (near) infrared photocatalytic behavior. *Journal of Materials Chemistry* 2012; 22(34): 17470–17475.
12. Zhang Y, Liang Y, Zhou J. Recent progress of graphene doping. *Acta Chimica Sinica* 2014; 72(3): 367–377.
13. Shen C, Zhang J, Shi D, *et al.* Photoluminescence enhancement in monolayer molybdenum disulfide by annealing in air. *Acta Chimica Sinica* 2015; 73(9): 954–958.
14. Shi J, Ma D, Zhang Y, *et al.* Controllable growth of MoS<sub>2</sub> on Au foils and its application in hydrogen evolution. *Acta Chimica Sinica* 2015; 73(9): 877–885.
15. Chang K, Mei Z, Wang T, *et al.* MoS<sub>2</sub>/graphene cocatalyst for efficient photocatalytic H<sub>2</sub> evolution under visible light irradiation. *ACS Nano* 2014; 8(7): 7078–7087.
16. Zong X, Wu G, Yan H, *et al.* Photocatalytic H<sub>2</sub> evolution on MoS<sub>2</sub>/CdS catalysts under visible light irradiation. *Journal of Physical Chemistry C* 2010; 114(4): 1963–1968.
17. Zong X, Yan H, Wu G, *et al.* Enhancement of photocatalytic H<sub>2</sub> evolution on CdS by loading MoS<sub>2</sub> as cocatalyst under visible light irradiation. *Journal of the American Chemical Society* 2008; 130(23): 7176–7177.
18. Yang L, Zhong D, Zhang J, *et al.* Optical properties of metal-molybdenum disulfide hybrid nanosheets and their application for enhanced photocatalytic hydrogen evolution. *ACS Nano* 2014; 8(7): 6979–6985.
19. Li Y, Wang H, Peng S. Tunable photodeposition of MoS<sub>2</sub> onto a composite of reduced graphene oxide

- and CdS for synergic photocatalytic hydrogen generation. *The Journal of Physical Chemistry C* 2014; 118(34): 19842–19848.
20. Xiang Q, Yu J, Jaroniec M. Synergetic effect of MoS<sub>2</sub> and graphene as cocatalysts for enhanced photocatalytic H<sub>2</sub> production activity of TiO<sub>2</sub> nanoparticles. *Journal of the American Chemical Society* 2012; 134(15): 6575–6578.
  21. Min S, Lu G. Sites for high efficient photocatalytic hydrogen evolution on a limited-layered MoS<sub>2</sub> cocatalyst confined on graphene sheets—The role of graphene. *Journal of Physical Chemistry C* 2012; 116(48): 25415–25424.
  22. Yin W, Yan L, Yu J, *et al.* High-throughput synthesis of single-layer MoS<sub>2</sub> nanosheets as a near-infrared photothermal-triggered drug delivery for effective cancer therapy. *ACS Nano* 2014; 8(7): 6922–6933.
  23. Mak KF, Lee CG, Hone J, *et al.* Atomically thin MoS<sub>2</sub>: A new direct-gap semiconductor. *Physical Review Letters* 2010; 105(13): 474–479.
  24. Noorden VR. Moving towards a graphene world. *Nature* 2006; 442(7100): 228–229.
  25. Stolyarova E, Rim KT, Ryu SM, *et al.* High-resolution scanning tunneling microscopy imaging of mesoscopic graphene sheets on an insulating surface. *Proceedings of the National Academy of Sciences of the United States of America* 2007; 104(22): 9209–9212.
  26. Novoselov KS, Geim AK, Morozov SV, *et al.* Two-dimensional gas of massless diracfermions in graphene. *Nature* 2005; 438(7065): 197–200.
  27. Tian Y, He Y, Shang J, *et al.* Hydrothermal synthesis and characterization of laminar MoS<sub>2</sub>. *Acta Chimica Sinica* 2004; 62(18): 1807–1810.
  28. Xu Y, Sheng K, Li C, *et al.* Self-assembled graphene hydrogel via a one-step hydrothermal process. *ACS Nano* 2010; 4(7): 4324–4330.
  29. Shen J, Li T, Long Y, *et al.* One-step solid state preparation of reduced graphene oxide. *Carbon* 2012; 50(6): 2134–2140.
  30. Zhou Y, Bao Q, Tang LAL, *et al.* Hydrothermal dehydration for the “green” reduction of exfoliated graphene oxide to graphene and demonstration of tunable optical limiting properties. *Chemistry of Materials* 2009; 21(13): 2950–2956.
  31. Wu H, Yang R, Song B, *et al.* Biocompatible inorganic fullerene-like molybdenum disulfide nanoparticles produced by pulsed laser ablation in water. *ACS Nano* 2011; 5(2): 1276–1281.
  32. Stankovich S, Dikin DA, Piner RD, *et al.* Synthesis of graphene-based nanosheets via chemical reduction of exfoliated graphite oxide. *Carbon* 2007; 45(7): 1558–1565.